

Elsevier Editorial System(tm) for Science of  
the Total Environment

Manuscript Draft

Manuscript Number: STOTEN-D-18-04473

Title: Pathways of inorganic and organic pollutants from land to deep sea: the case study of the Gulf of Cagliari (W Tyrrhenian Sea)

Article Type: Research Paper

Keywords: Tyrrhenian Sea, submarine canyons, deep sea, pollution focusing.

Corresponding Author: Dr. Stella Tamburrino, PhD

Corresponding Author's Institution:

First Author: Stella Tamburrino, PhD

Order of Authors: Stella Tamburrino, PhD; Salvatore Passaro; Mattia Barsanti; Antonio Schirone; Ivana Delbono; Fabio Conte; Roberta Delfanti; Maria Bonsignore; Marianna Del Core; Serena Gherardi; Mario Sprovieri

Abstract: Dynamics of pollutants from land to deep sea have been investigated in a pilot area of the central Mediterranean basin (Gulf of Cagliari, S Sardinia) where important industrial plants are sited since beginning of the last century. The deep-sea (>200 m) has long been considered a pristine environment due to its remoteness from anthropogenic pollution sources. Nonetheless, in continental margins, canyons appear to act as natural conduits of sediments and organic matter from the shelf to deep basins, providing an efficient physical pathway for transport and accumulation of particles with their associated land-produced contaminants. The continental slope of the south Sardinia has been used as a natural laboratory for investigating mechanisms and times of transfer dynamics of contaminants from land to sea and from shelf and deep sea through an articulated system of submarine canyons. Five sediment cores dated by  $^{210}\text{Pb}$  and  $^{137}\text{Cs}$  reveal: i) a complex dynamics of organic and inorganic pollutants from point source areas on land to the deep sea and ii) a crucial role played by canyons and bottom morphology as primary pathway conveying sediments and associated contaminants from sources to very far deep sea environments. This study unequivocally suggests that land and deep sea appear much more connected than previously assumed. This is challenging mostly in regions where coastal pollution could represent critical threats for larger areas of the Mediterranean Sea.

Suggested Reviewers: Leonardo Langone  
ISMAR-CNR  
leonardo.langone@ismar.cnr.it

Milena Horvat  
Jozef Stefan Institute, Department of Environmental Sciences, Slovenia  
milena.horvat@ijs.si

Ana Carolina Ruiz-Fernandez  
Unidad Académica Mazatlán, Instituto de Ciencias del Mar y Limnología,  
Universidad Nacional Autónoma de México, Mazatlán, Sinaloa, Mexico  
caro@ola.icmyl.unam.mx

Ethel Eljarrat  
CSIC - Instituto de Diagnostico Ambiental y Estudios del Agua (IDAEA),  
Department of Environmental Chemistry, Spain  
eeeqam@iiqab.csic.es

Miriam Diamond  
Univerisity of Toronto  
miriam.diamond@utoronto.ca

Opposed Reviewers:



**To the kind attention of the  
Editor of the Science of the Total Environment**

Dear Editor,  
here enclosed you find the manuscript entitled  
**“Pathways of inorganic and organic pollutants from land to deep sea: the case study of the Gulf of Cagliari (W Tyrrhenian Sea)”**

By *Stella Tamburrino*, Salvatore Passaro, Mattia Barsanti, Antonio Schirone, Ivana Delbono, Fabio Conte, Roberta Delfanti, Maria Bonsignore, Marianna Del Core, Serena Gherardi and Mario Sprovieri

that we would like to submit to the Science of the Total Environment.

The results presented in the manuscript have not been published elsewhere and they have been not submitted to other journals. An abstract (“*Contaminants transfer from land to the deep sea: processes and dynamics from the case study of the Gulf of Cagliari (W Tyrrhenian Sea)*”) has been presented to the EGU 2018 Congress, where we reported only preliminary results from this study.

All authors are aware of and accept responsibility for the manuscript.

The geochemical and geophysical data were obtained through advanced analytical methods and they aim to provide a high-quality database useful to investigate dynamics of contaminants from land to sea. Furthermore we retain that this paper may represent a pilot study suitable for researchers interested both on coastal management of the Tyrrhenian region, and on exploring mechanisms and timing of transfer dynamics of contaminants from land to sea and from shelf to deep-sea through articulated system of submarine canyons.

We hope that the topic is interesting and suitable for the journal. I thank you in advance and hoping to hear from you soon I give you my best regards.

Corresponding author:

**Stella Tamburrino**

Institute for Coastal and Marine Environment (IAMC) – CNR  
Calata Porta di Massa, Porto di Napoli, 80133, Napoli, Italy  
stella.tamburrino@iamc.cnr.it  
Phone (+39) 081 5423832, Fax (+39) 081 5423888

Sincerely

**Stella Tamburrino**

1  
2  
3  
4 **Pathways of inorganic and organic pollutants from land to deep sea: the case study of the Gulf**  
5 **of Cagliari (W Tyrrhenian Sea)**

6 Stella Tamburrino<sup>a</sup>, Salvatore Passaro<sup>a</sup>, Mattia Barsanti<sup>b</sup>, Antonio Schirone<sup>b</sup>, Ivana Delbono<sup>b</sup>, Fabio  
7 Conte<sup>b</sup>, Roberta Delfanti<sup>b</sup>, Maria Bonsignore<sup>c</sup>, Marianna Del Core<sup>c</sup>, Serena Gherardi<sup>a</sup>, Mario  
8 Sprovieri<sup>c</sup>

9 a) IAMC-CNR Calata Porta di Massa, Napoli, Italy

10 b) ENEA Centro Ricerche Ambiente Marino S. Teresa, La Spezia, Italy

11 c) IAMC-CNR SS Via Del Mare 3, Torretta-Granitola Campobello di Mazara (TP) Italy

12  
13  
14 **Corresponding author**

15 Stella Tamburrino

16 IAMC-CNR Calata Porta di Massa, Napoli, Italy

17 Phone + 39 081 5423832

18 Fax + 39 081 5423888

19 e-mail: [stella.tamburrino@iamc.cnr.it](mailto:stella.tamburrino@iamc.cnr.it)

20  
21  
22  
23  
24 **Abstract**

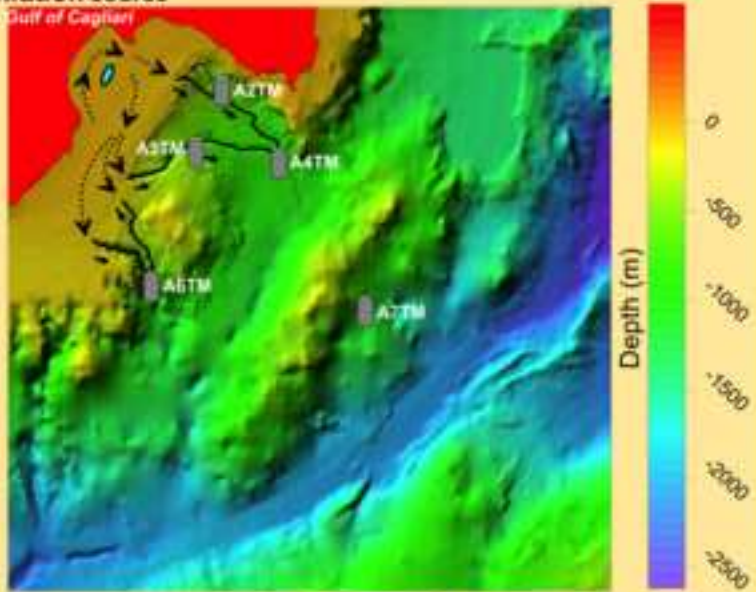
25 Dynamics of pollutants from land to deep sea have been investigated in a pilot area of the central  
26 Mediterranean basin (Gulf of Cagliari, S Sardinia) where important industrial plants are sited since  
27 beginning of the last century. The deep-sea (>200 m) has long been considered a pristine  
28 environment due to its remoteness from anthropogenic pollution sources. Nonetheless, in  
29 continental margins, canyons appear to act as natural conduits of sediments and organic matter  
30 from the shelf to deep basins, providing an efficient physical pathway for transport and  
31 accumulation of particles with their associated land-produced contaminants. The continental  
32 slope of the south Sardinia has been used as a natural laboratory for investigating mechanisms  
33 and times of transfer dynamics of contaminants from land to sea and from shelf and deep sea  
34 through an articulated system of submarine canyons. Five sediment cores dated by <sup>210</sup>Pb and <sup>137</sup>Cs  
35 reveal: i) a complex dynamics of organic and inorganic pollutants from point source areas on land  
36 to the deep sea and ii) a crucial role played by canyons and bottom morphology as primary  
37 pathway conveying sediments and associated contaminants from sources to very far deep sea  
38 environments. This study unequivocally suggests that land and deep sea appear much more  
39 connected than previously assumed. This is challenging mostly in regions where coastal pollution  
40 could represent critical threats for larger areas of the Mediterranean Sea.

41  
42  
43  
44  
45  
46  
47 **Key words**

48 Tyrrhenian Sea, submarine canyons, deep sea, pollution focusing

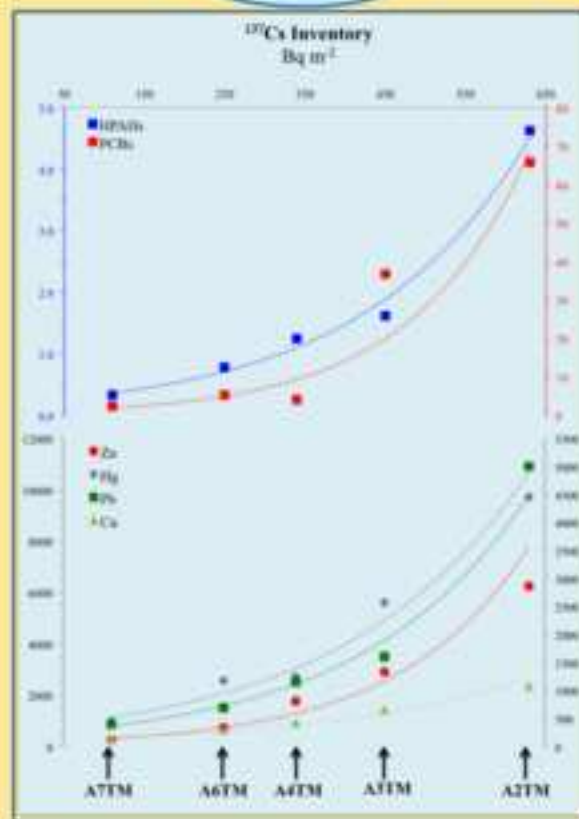
49  
50  
51  
52  
53  
54  
55  
56  
57  
58  
59  
60  
61  
62  
63  
64  
65

**Pollution source**



Coastal to deep-sea disposal of contaminants

**Inventories of pollutants**





## Highlights

- Five sedimentary records from the Gulf of Cagliari (W Tyrrhenian Sea) document anthropogenic impacts in the deep sea
- Bottom morphology reveals a complex and articulated system of submarine canyons
- Geochemical analyses: inorganic and organic compounds, radionuclide measurements
- Dynamics of contaminants from land to sea and from shelf to deep sea
- Pilot study to identify canyons as primary pathway conveying sediments and associated contaminants from sources to very far deep sea environments

1 **Pathways of inorganic and organic pollutants from land to deep sea: the case study of**  
2 **the Gulf of Cagliari (W Tyrrhenian Sea)**

3  
4 Stella Tamburrino<sup>a\*</sup>, Salvatore Passaro<sup>a</sup>, Mattia Barsanti<sup>b</sup>, Antonio Schirone<sup>b</sup>, Ivana Delbono<sup>b</sup>,  
5 Fabio Conte<sup>b</sup>, Roberta Delfanti<sup>b</sup>, Maria Bonsignore<sup>c</sup>, Marianna Del Core<sup>c</sup>, Serena Gherardi<sup>a</sup>,  
6 Mario Sprovieri<sup>c</sup>

7  
8 a) IAMC-CNR Calata Porta di Massa, Napoli, Italy

9 b) ENEA Centro Ricerche Ambiente Marino S. Teresa, La Spezia, Italy

10 c) IAMC-CNR SS Via Del Mare 3, Torretta-Granitola Campobello di Mazara (TP) Italy

11  
12 \* Phone + 39 081 5423832; Fax + 39 081 5423888; e-mail: [stella.tamburrino@iamc.cnr.it](mailto:stella.tamburrino@iamc.cnr.it)

13  
14  
15 **Abstract**

16 Dynamics of pollutants from land to deep sea have been investigated in a pilot area of the  
17 central Mediterranean basin (Gulf of Cagliari, S Sardinia) where important industrial plants  
18 are sited since beginning of the last century. The deep-sea (>200 m) has long been considered  
19 a pristine environment due to its remoteness from anthropogenic pollution sources.  
20 Nonetheless, in continental margins, canyons appear to act as natural conduits of sediments  
21 and organic matter from the shelf to deep basins, providing an efficient physical pathway for  
22 transport and accumulation of particles with their associated land-produced contaminants.  
23 The continental slope of the south Sardinia has been used as a natural laboratory for  
24 investigating mechanisms and times of transfer dynamics of contaminants from land to sea  
25 and from shelf and deep sea through an articulated system of submarine canyons. Five

26 sediment cores dated by  $^{210}\text{Pb}$  and  $^{137}\text{Cs}$  reveal: i) a complex dynamics of organic and  
27 inorganic pollutants from point source areas on land to the deep sea and ii) a crucial role  
28 played by canyons and bottom morphology as primary pathway conveying sediments and  
29 associated contaminants from sources to very far deep sea environments. This study  
30 unequivocally suggests that land and deep sea appear much more connected than previously  
31 assumed. This is challenging mostly in regions where coastal pollution could represent critical  
32 threats for larger areas of the Mediterranean Sea.

33

#### 34 **Key words**

35 Tyrrhenian Sea, submarine canyons, deep sea, pollution focusing

36

#### 37 **1 Introduction**

38 Coastal marine areas are under increasing pressure due to various anthropogenic activities  
39 with their relevant input of pollutants to the sea and consequent concerns for the fragile  
40 marine ecosystems. The complex biogeochemistry of inorganic and organic contaminants in  
41 the marine environment combined to their persistence and limited potential for degradation,  
42 produces long-term residence time, long-range potential transport and relevant effects of  
43 bioaccumulation and biomagnification in the trophic web (e.g., Lohmann et al., 2007;  
44 Scheringer et al., 2009). Pollutants in the marine sediments undergo a combination of  
45 chemical (e.g., adsorption/desorption, water/particle exchanges, etc.), early diagenetic and  
46 sedimentological processes (e.g., re-suspension and re-deposition), which make difficult to  
47 track, in terms of chemical and physical dynamics, their evolution in the marine environment.  
48 Recent investigations demonstrated that many chemical pollutants reach the deep-sea (e.g.  
49 Storelli et al., 2009; Jamieson et al., 2017) representing, with the reduced physical and  
50 chemical dynamics of this environment, a long-term risk with unpredictable effects for the



51 deep ecosystem (Froescheis et al., 2000; Covaci et al., 2008). The deep-sea (>200 m) has long  
52 been considered a pristine environment due to its remoteness from anthropogenic sources.  
53 Nevertheless, in continental margins, canyons act as natural conduits of sediments and  
54 organic matter from the shelf to the deep basins, providing an efficient physical pathway for  
55 transport and accumulation of particles with associated land-produced pollutants. Several  
56 recent multidisciplinary projects have focused on the study of canyons, and have considerably  
57 increased our understanding of their ecological role, the goods and services they provide to  
58 humans, and the impacts that anthropogenic activities have on their ecological condition  
59 (Fernandez-Arcaya et al., 2017). Being a link between coastal areas and deep oceans, they  
60 serve as conduits for the transport of sedimentary material from the surface to the bottom of  
61 the sea (Fabres et al., 2008). Also, the role played by canyons in transporting pollutants to the  
62 deep sea is enormously reinforced when they are the locations of highly dynamic shelf to  
63 basin export processes (i.e. Dense Shelf Water Cascading-DSWC in the NW Mediterranean Sea;  
64 Canals et al., 2006). In this context, the continental slope of the south Sardinia is an interesting  
65 natural laboratory for exploring mechanisms and timing of transfer dynamics of contaminants  
66 from land to sea and from shelf to deep-sea through an articulated system of submarine  
67 canyons and specific source areas. An ensemble of chemical analyses of radionuclides,  
68 inorganic and organic compounds from sediment cores sampled from coastal to deep-sea  
69 areas provide a unprecedented opportunity to investigate dynamics of contaminants from the  
70 land sources to the marine sinks.

71

## 72 **2 Site description**

73 The Gulf of Cagliari (CG) is placed in the SE sector of Sardinia (Figure 1A), where fluvial  
74 sedimentation since Pleistocene caused favourable conditions for the development of coastal  
75 lagoons separated by the rhodalgal limestones Miocenic hills of Cagliari (Cossellu et al., 2006;

76 Kalb et al., 2008). Holocenic sandbars complete the evolution of the coastal margin. Clayey,  
77 sand and siliciclastic carbonate sediments characterize the latest Pleistocene-Holocene  
78 stratigraphy of Cagliari Basin. Because of sediment supply, sea-level changes and tectonics, CG  
79 has a pronounced shelf that extends about 15-20 km south-eastward (Lecca et al., 1998). The  
80 shelf abruptly interrupts with a marked break in slope located at 60/80 m below sea level  
81 (bsl). Extensive canyons (and several tributary incisions) dissect the offshore-continental  
82 slope margin of CG, named Pula (PC), Sarroch (SC), S. Elia-Foxi (SEC) and Carbonara (CC),  
83 respectively (Figure 1B). In this area, also two major seafloor relative highs are present: the  
84 Carbonara Ridge (CR) and the Banghittu Knoll (BK; Figure 1B and 1C). CR is a 85 km long, 25  
85 km wide NE-SW striking seamount rising more than 1000 m from the surrounding seafloor  
86 (Figure 1C). The deeper flanks of CR slopes are located at 1250 m bsl, while its apical sector  
87 reaches 156 m bsl. BK is located in the SW sector of CG, on the uppermost portion of the slope,  
88 where it acts as a physiographic boundary between SC and PC. BK shows an almost flat, SW  
89 gently dipping top (ca 0.5°) on its apical part, which is located between 110/140 m bsl.  
90 The presence of two major industrial complexes dominate potential inputs of contaminants at  
91 sea from the coastal area of the CG: the major and industrial area of the Cagliari town and, in  
92 the westernmost part of the gulf, the refinery industrial plant of Sarlux-Saras (Figure 1).

93

### 94 **3 Data and methods**

95 Seafloor bathymetry and sediment cores were acquired during the Anomcity\_2014  
96 oceanographic cruise on-board of the R/V Minerva Uno (National Research Council, CNR).  
97 Bathymetric data were used to deploy a Digital Terrain Model (DTM) covering an area of  
98 17'000 km<sup>2</sup> in the 2670 m to 1 m bsl bathymetric range.

99 Five sediment cores were collected using a box-corer, at depths ranging from 475 and 1153 m  
100 (Figure 1A and 1B; Table 1). The A2TM and A3TM cores are located at a depth of about 600 m

101 bsl in the SEC and SC canyon branches, respectively; these two sampling sites were selected  
102 where a slope decrease in the seafloor morphology has been observed. The A4TM sets at the  
103 confluence of SEC and SC active branches, at a depth of about 900 m bsl, while the A6TM was  
104 sampled at the confluence of the PC active branches (SW from A2TM and A3TM, at about 780  
105 m bsl). Finally, the A7TM lies SE from the apical sector of the CR main axis, at about 1140 m  
106 bsl depth. Core sub-samples were prepared for grain size, geochemical and radiometric  
107 analyses. Cores analysis included: radionuclide measurements, grain-size fraction,  
108 concentrations of Al, Fe, Mn, Cd, Pb, Co, V, As, Cr, Cu, Ni, Zn, Hg, TOC, TN, PAHs (16 US-EPA  
109 priority congeners) and  $\Sigma$ PCBs. Results are reported in Supplementary Table S1. A full  
110 description of data and methods can be found in the additional materials (see text in  
111 Supplementary Material).

112

## 113 **4 Results**

114

### 115 **4.1 Seafloor morphology**

116 The morphology shows the existence of several abandoned canyon branches, partially filled  
117 by sediments and presently unlinked to the active sections of SC and SEC (Figure 1B).  
118 Contrary to the active canyon thalwegs, minor incisions tend to disappear toward deeper  
119 sectors of the slope. Since their intrinsic sediment dynamic, the CG active set of canyons and  
120 incisions rules the mechanism of sediment distribution from land to deep sea (e.g., Puig et al.,  
121 2014). The overall emplacement of uppermost branches of canyons is mainly controlled by  
122 the slope direction, i.e., ca NW-SE (Figure 1B and 1C). On the contrary, the presence of CR,  
123 located at the slope foot, constraints the pattern of deeper segments of canyons (Figure 1B).

124

### 125 **4.2 Radionuclide tracers and chronology**

126 The combined use of  $^{210}\text{Pb}$  and  $^{137}\text{Cs}$  profiles provides a solid based geochronology during the  
127 last century, since these elements have similar half-lives (22.23y and 30.05y, respectively) but  
128 quite different inputs in the environment: natural  $^{210}\text{Pb}$  is continuously produced by its  
129 parents while artificial  $^{137}\text{Cs}$  is time dependent (Hancock et al., 2000; Smith, 2001). In fact,  
130  $^{137}\text{Cs}$  has been diffused in the environment mainly during the nuclear tests in atmosphere in  
131 the 1945-1963 period and then reached an ubiquitous distribution. In the marine  
132 environment, a large fraction of radionuclides and pollutants is associated with particles and  
133 fine sediments (Baskaran et al., 1993; van Wijngaarden et al., 2002 and reference therein)  
134 settling through the water column and reaching the seafloor. Therefore, high deposition of  
135  $^{137}\text{Cs}$  marks sites with high accumulation of recent fine particles.

136  $^{210}\text{Pb}$  and  $^{137}\text{Cs}$  downcore profiles in the five sediment cores of this study are shown in  
137 Supplementary Figure S1. The A2TM and A3TM cores (SI Figure S1A and S1B) show a clearly  
138 visible  $^{137}\text{Cs}$  sub-surface peak in the downcore activity profiles. At station A2TM, assuming a  
139 Constant Flux of  $^{210}\text{Pb}$  and a Constant Sedimentation rate (CF:CS model) (Appleby, and  
140 Oldfield, 1992; Robbins, 1978) in the last century, a Mass Accumulation Rate (MAR) of  $0.24 \pm$   
141  $0.01 \text{ g/cm}^2 \text{ y}$ , equivalent to a Sediment Accumulation Rate (SAR) of  $0.33 \pm 0.01 \text{ cm/y}$ , is  
142 calculated. With this MAR value, the  $^{137}\text{Cs}$  sub-surface peak (mass depth =  $12.3 \text{ g/cm}^2$ )  
143 corresponds to the year  $1963 \pm 2$ , in perfect agreement with the real maximum fallout  
144 deposition in 1963. Furthermore,  $^{137}\text{Cs}$  disappears below  $16,27 \text{ g/cm}^2$ , dated back to  $1946 \pm 2$ ,  
145 very close to the beginning of the nuclear weapons testing. Consequently, the  $^{210}\text{Pb}$  dating for  
146 the A2TM core is considered to be totally reliable and accurate. Differently for station A3TM,  
147 MAR calculated by the CF:CS model from the  $^{210}\text{Pb}$  downcore profile is  $0.18 \pm 0.01 \text{ g/cm}^2 \text{ y}$   
148 (equal to a SAR of  $0.26 \pm 0.02 \text{ cm/y}$ ). This dates the  $^{137}\text{Cs}$  peak (mass depth =  $6.5 \text{ g/cm}^2$ ) at  
149  $1978 \pm 3$ , which is not consistent with the  $^{137}\text{Cs}$  global fallout peak in 1963. If we assume a  
150 variable sedimentation rate and apply the Constant Rate of Supply (CRS) model (Appleby, and

151 Oldfield, 1978) to the  $^{210}\text{Pb}$  activity profile, the  $^{137}\text{Cs}$  peak dating improves with the result of  
152 the year  $1956 \pm 5$ , closer to the 1963 peak. With the CRS calculation, the  $^{210}\text{Pb}$  dating of the  
153 A3TM core is more reliable although it shows a greater uncertainty than the A2TM core. The  
154 use of two different models highlights a different nature in terms of sedimentary dynamics of  
155 SEC and SC Canyons where the A2TM and A3TM cores are located, respectively.

156 For the other three sediment cores (A4TM, A6TM and A7TM),  $^{210}\text{Pb}$  and  $^{137}\text{Cs}$  downcore  
157 activity profiles (SI Figure S1C, S1D and S1E) are more disturbed because of post-depositional  
158 processes such as bioturbation and sediment mixing. Furthermore,  $^{137}\text{Cs}$  activity profile does  
159 not allow a validation of the  $^{210}\text{Pb}$ -based dating models and no reliable dating is available for  
160 sediment cores A4TM, A6TM and A7TM.

161

### 162 **4.3 Grain size, inorganic and organic geochemistry of sediments: trends and potential** 163 **sources of pollution**

164 Some relevant features emerge, particularly in the two cores A2TM and A3TM, which reveal in  
165 great detail some of the most important and historically documented anthropogenic impacts  
166 on the near coast during the last 110 years. In particular, in the A2TM core,  $\Sigma\text{PAHs}$ , Pb and Hg  
167 increase since 1930, testifying the first industrial activities already well documented for the  
168 Cagliari industrial area (Figure 2A).  $\Sigma\text{PCBs}$  have been detected since 1940, immediately after  
169 the industrial use of these chemicals in Italian chemical plants. Also, three time intervals  
170 1900-1940, 1940-1980, 1980-recent well document (particularly in the A2TM core), in terms  
171 of gradually increasing silty fraction (see box plot at the bottom of the Figure 2A), the effects  
172 of anthropogenic damming on land which progressively reduced input of sediments fine  
173 fraction at sea. The  $\Sigma\text{PCBs}$  profile in the A3TM core shows a similar behaviour with As and Hg  
174 increasing only since 1960, thus reflecting the start-up of industrial activity in the Sarlux-  
175 Saras refinery (Figure 2B). Thus, these two sediment cores document with high accuracy the

176 most important anthropogenic events on land with different spatial responses to the two  
177 diverse point sources.

178 The A4TM core clearly reflects, considering the last ~110 years, anthropogenic inputs from  
179 land of  $\Sigma$ PCB,  $\Sigma$ PAHs, Pb, Hg and As, thus documenting an efficient transport and  
180 accumulation in the sediments (Figure 2C). Although documented in a shorter sedimentary  
181 record, the input of anthropogenic contaminants ( $\Sigma$ PAHs,  $\Sigma$ PCBs, As and Pb) is identified in  
182 the last ~110 years of the A6TM core (Figure 2D). Noteworthy, significant amounts of  $\Sigma$ PCBs  
183 and minor of  $\Sigma$ PAHs, Co, Cr, Ni, V and Zn were also found in the upper part of the A7TM,  
184 characterised by extremely low sedimentation rate (Figure 2E).

185

#### 186 **4.4 Inventory of pollutants and patterns of distribution**

187 The estimate of the inventories for the anthropogenic contribution of each single Trace  
188 Element (hereafter TE) in each sediment core layer was calculated firstly by subtracting the  
189 percentage related to the different mineralogical and background components from the total  
190 concentration of the TE and then by multiplying by the mass depth value estimated for each  
191 sample. More in detail, in order to minimize the contribution of grain size and mineralogy on  
192 the concentration of each TE in the sediments and thus estimate the anthropogenic  
193 component, we subtracted the percentage calculated as TE/Al ratio from each point with  
194 respect to the minimum TE/Al documented in each core. On the other hand, background  
195 values for  $\Sigma$ PAHs and  $\Sigma$ PCBs were calculated as the lowest concentration value documented  
196 in the lowermost part of the five cores. Then, for each TE, including  $^{137}\text{Cs}$ , the inventory was  
197 calculated as cumulative sum of the concentrations in each sediment layer multiplied by its  
198 bulk dry density and divided by the core surface area (Table 2).

199

## 200 **5 Discussion**

201

## 202 **5.1 Radionuclides as tracers for sediment transport**

203 The levels and the downcore distribution of natural and anthropogenic radionuclides can be  
204 used to derive information about the sediment provenance and composition (Ra isotopes and  
205  $^{40}\text{K}$ ) and to characterize depositional environments and sediment accumulation rates ( $^{210}\text{Pb}$ ,  
206  $^{137}\text{Cs}$ ).

207 The balance of  $^{210}\text{Pb}$ xs fluxes ( $\text{Bq m}^{-2} \text{y}^{-1}$ ) at the sediment-water interface is shown for each  
208 station in the Supplementary Figure S2.  $^{210}\text{Pb}$ xs flux accumulated in sediments ( $F_s$ ) exceeds  
209 the estimated flux from atmospheric deposition ( $F_a$ ) and decay of  $^{226}\text{Ra}$  in the water column  
210 ( $F_m$ ), with the exception of A7TM. In detail, A2TM shows the strongest lateral transport of  
211  $^{210}\text{Pb}$ xs, and the  $^{210}\text{Pb}$ xs profile of the A2TM station indicates a regular and constant  
212 sedimentation over a  $\sim 110$  year time scale. These features are in agreement with (Meleddu et  
213 al., 2016) which identify hyperpycnal flows in the northern area of CG that, considering the  
214 limited extension of the continental shelf, influence the development of deposits in the head of  
215 the SEC (Figure 1B).  $^{210}\text{Pb}$ xs data of A2TM core identify a sediment deposition transported by  
216 these hyperpycnal flows pointing out the constant SEC sediment transport activity.

217 Similarly to A2TM, A3TM station shows a significant lateral input of  $^{210}\text{Pb}$ xs but displays a  
218 more disturbed trend of  $^{210}\text{Pb}$ xs profile. These observations support the hypothesis made in  
219 the CRS model obtained by data (see previous chronology section), thus suggesting a variable  
220 sedimentation supply for A2TM and A3TM on the basis of the  $^{210}\text{Pb}$ xs profiles. The obtained  
221 result is substantially in agreement with (Orrù et al., 2014), that mapped two significant  
222 marine slide deposits located in correspondence of Sarroch. These deposits extend from the  
223 edge of the continental shelf to a depth of about 400 m (until the head of SC). Moreover they  
224 are affected by erosion in the SC, causing a less regular deposition at A3TM than at A2TM.  
225 Although, A3TM is located at the same depth of A2TM, its  $^{210}\text{Pb}$ xs surface activity is about half

226 of A2TM, thus indicating that the A3TM station receives a relevant sediment input from these  
227 marine slide deposits.

228 A4TM and A6TM are quite similar and show a lower lateral supply of  $^{210}\text{Pb}_{\text{xs}}$ . However,  
229  $^{210}\text{Pb}_{\text{xs}}$  fluxes are twice the expected ones by considering the atmospheric and the seawater  
230 contributions only, thus indicating a significant supply of sedimentation.

231 Differently, the A7TM core (the deepest one) shows a globally lower  $^{210}\text{Pb}_{\text{xs}}$  flux than the  
232 expected. Here the post-depositional are dominant compared to sedimentation rate values,  
233 very similar to those of the deep sea. Since the CR separate A7TM from the slope, this latter is  
234 poorly interested by sedimentation arising by the shelf and the slope, while is subjected to  
235 other marine sources of sediments as testified by  $^{40}\text{K}$ ,  $^{234}\text{Th}$  and grain size data (SI Table S2  
236 and Figure S4).

237

## 238 **5.2 Inventories of contaminants and sediment patterns distribution**

239 Despite  $^{137}\text{Cs}$  in the oceanic water column behaves as a soluble nuclide and hence  $^{137}\text{Cs}$  has  
240 properties that make it useful as a water mass tracer, a very little of  $^{137}\text{Cs}$  delivered to the  
241 ocean reaches the seabed. At present, there is no global fallout of  $^{137}\text{Cs}$  derived from nuclear  
242 weapons testing (Baskaran, 2011). The dominant source of  $^{137}\text{Cs}$  in the air is a re-suspension  
243 (e.g. due to agricultural activities) of previously deposited  $^{137}\text{Cs}$  in soil and its subsequent  
244 transport by winds (Pham et al., 2013 and references therein). Therefore,  $^{137}\text{Cs}$  can be reliably  
245 applied as tracer of terrigenous inputs of fine sediment fraction in coastal areas.

246 The Cagliari urban area, with its harbour and lagoon, represents the major source point for  
247 sediment release in the CG. Taking into account that, we infer a potential relationship between  
248 the distance of each sampling station from Cagliari and  $^{137}\text{Cs}$  inventories. Specifically, the  
249 inventory of  $^{137}\text{Cs}$  has been reported in Figure 3: i) against the linear distance estimated from  
250 the main source area (Cagliari; Figure 3A and 3B) and ii) against the estimated morphological



251 distance (following the thalweg of the canyon systems located in front of the two major  
252 industrial plants of Cagliari and Sarlux-Saras; Figure 3C and 3D) from land. The plot of  $^{137}\text{Cs}$   
253 inventories from each core vs the linear distances from the nearest coastline measured for  
254 each sample station shows a relatively low fit (Figure 3B). This plot testifies that  $^{137}\text{Cs}$  “travels”  
255 from land-to-sea but does not follow the ideal linear connection from a point to the nearest  
256 emerged sectors. Conversely, if we calculate a “morphological distance” from land, assuming  
257 that sediments travel from the shelf to the station following the preferential way of the axis of  
258 canyons, we obtain values that are in very closer relation with the  $^{137}\text{Cs}$  inventories (Figure  
259 3C) with a second order fitting line perfectly approximating the distribution of the four values.  
260 Really, the relationship between the “morphological distance” and the  $^{137}\text{Cs}$  inventories  
261 should be considered as the first part of an exponential decrease, since this trend must reach  
262 an equilibrium value for high distance from the coast, where the only source has been the  
263 direct fallout. Hence, by subtracting the A7TM inventory to other  $^{137}\text{Cs}$  inventories we can  
264 observe the distribution of  $^{137}\text{Cs}$  with terrigenous origin (Figure 4). This could suggest that  
265 coastal to deep-sea transport of sediments deposited at seafloor is strongly driven by  
266 morphology and drifting mechanism. Actually, once arrived at the break in slope, sediments  
267 undergone an acceleration and a re-disposing primarily driven by the gravity action of the  
268 over solid-flows on the slope. In addition, they are under the effects of the attractive action  
269 played by canyon axis. In this sense, local morphology plays a major role for sediment  
270 distribution, especially for channels and canyons for which the overall dynamic of sediment  
271 transport is quite faster with respect to the slope activity (SI Figure S3). It is worth stressing  
272 that submarine canyons act as preferential pathway for transport of sediment from the shelf  
273 to adjacent basins (e.g., Shepard, 1981), thus strongly influencing the evolution of the shelf  
274 itself and the overall sediment displacement of a slope (Canals et al., 2004; 2006; Allen et al.,  
275 2009; Piper and Normark, 2009; Puig et al., 2014; 2017; Talling, 2014). Presently, the

276 transport activity and the exchange of sediments with the upper, adjacent, external  
277 continental shelf seems to be primarily linked to the tectonic activity and the sediment supply  
278 from land. The sediment amount in the uppermost section of the shelf, as a result of  
279 anthropogenic activities (e.g., dredging of harbours or natural event like flash floods, etc.),  
280 may result in a re-activation of sediment transport along the canyon (Carter et al., 2012;  
281 Khripounoff et al., 2012; Puig et al., 2014). This implies that canyons, particularly those  
282 located in area characterized by important tectonic activity, may represent efficient focusing  
283 systems for pollutants from land (see Micallef et al., 2014 and reference therein). Then, once  
284 sediments reach break in slope, they are partially attracted from not incised slopes, partially  
285 by not active channel segments or abandoned canyons and, perhaps goes to fill old valleys.  
286 The calculated TE inventories for the different cores show comparable exponential decrease  
287 with the distance from land (considering the  $^{137}\text{Cs}$  as a reliable tracer; Figure 5) but the slope  
288 of this decrease is different for each element, reflecting specific geochemical affinity  
289 (sediment–water distribution coefficients,  $K_d$ ) with sediments (IAEA, 2004). The  $\Sigma\text{PAHs}$ -  
290  $\Sigma\text{PCBs}$  group shows an analogue behavior although a slightly more complex trend does not  
291 exclude other  $\Sigma\text{PAHs}$  and  $\Sigma\text{PCBs}$  sources and deposition mechanisms from the coastal area.  
292 In this study, we documented very fine correlations of sedimentological and chemical features  
293 among dated cores located at different depths and morphologic settings. A primary control of  
294 contaminants transport from land to the deep sea via shelf canyons could represent a  
295 systematic mechanism of contaminants focusing generating hot spots of pollutants in the  
296 uncontaminated ocean sediments from very far point sources on land. Transport mechanisms  
297 by shelf canyons could offer unforeseen fast track system of deep sea contamination. A  
298 dominant geomorphological feature of the Mediterranean basin in terms of shelf-to-deep sea  
299 connection is represented by innumerable canyons, which document geological events  
300 modelling the mid- to long-term regional events. These canyons represent natural conduit

301 conveying sediments and associated contaminants from sources on land to very far deep sea  
302 environments. Thus, land and deep sea appear much more connected than previously  
303 assumed in a region where coastal pollution represents a crucial threat for large areas of the  
304 Mediterranean Sea.

305

### 306 **Supplementary Material**

307

308 Additional Information regarding materials and methods are detailed described and shown  
309 in Figure S1-S4 and Table S1-S2.

310

### 311 **Acknowledgments**

312

313 Financial support to this research was provided by the Italian Flagship Project RITMARE  
314 (MIUR-CNR). We thank the R/V Minerva Uno crewmembers for the active collaboration and  
315 help during all operations on board.

316

### 317 **References**

318

319 Allen, E.; Durrieu de Madron, X.; 2009. A review of the role of submarine canyons in deep-  
320 ocean exchange with the shelf. *Ocean Sci.*, 5, 607-620.

321 Aller, R.C.; Cochran, J.K.; 1976.  $^{234}\text{Th}/^{238}\text{U}$  disequilibrium in near-shore sediment: particle  
322 reworking and diagenetic time scales. *Earth and Planetary Science Letters*, 29, pp. 37-50.

323 Appleby, P.G.; Oldfield, F.; 1978. The calculation of lead-210 dates assuming a constant rate of  
324 supply of unsupported  $^{210}\text{Pb}$  to the sediment. *Catena* 5, 1-8.

325 Appleby, P.G.; Oldfield, F.; 1992. Application of lead-210 to sedimentation studies, in:  
326 Ivanovich, M., Harman, R.S. (Eds.), Uranium-Series Disequilibrium: Application to Earth,  
327 Marine, and Environmental Sciences. Clarendon Press, Oxford.

328 Baskaran, M.; 2011. Handbook of Environmental Isotope Geochemistry, Media, Advances in  
329 Isotope Geochemistry. Springer.

330 Baskaran, M.; and Santschi, P. H.; 1993. The role of particles and colloids in the transport of  
331 radionuclides in coastal environments of Texas. Mar. Chem. 43,95-114.

332 Basso, D.; Thomson, J.; Corselli, C.; 2004. Indications of low macrobenthic activity in the deep  
333 sediments of the eastern Mediterranean Sea 68, 53–62. doi:10.3989/scimar.2004.68s353.

334 Canals M.; Puig P.; Durrieu de Madron X.; Heussner S.; Palanques A.; Fabrés J.; 2006. Flushing  
335 submarine canyons. Nature, 444 , 354-357.

336 Canals, M.; Casamor J.L.; Lastras G.; Monaco A.; Acosta J.; Berné S.; Loubrieu B.; Weaver P.P.E.;  
337 Grehan A.; Dennielou B.; 2004. The role of canyons on strata formation. Oceanography, 17, 80-  
338 91.

339 Canals, M.; Puig, P.; Durrieu de Madron X.; Heussner, S.; Palanques, A.; Fabrés, J.; 2006.  
340 Flushing submarine canyons. Nature, 444, 354-357.

341 Carroll, J.; Lerche, I., 2003. Sedimentary Processes: Quantification Using Radionuclides.  
342 Elsevier, Oxford.

343 Carter, L.; Milliman, J.D.; Talling, P.J.; Gavey, R.; Wynn, R.B.; 2012. Near-synchronous and  
344 delayed initiation of long run-out submarine sediment flows from a record-breaking river  
345 flood, offshore Taiwan. Geophys. Res. Lett., 39, Article L12603.

346 Cossellu, M.; 2007. Sedimentologia e processi deposizionali della piattaforma continentale di  
347 Cagliari dal Last Glacial Maximum all'attuale. PhD Thesis, Università degli Studi di Cagliari, pp.  
348 218.

349 Covaci, A.; Losada, S.; Roosens, L.; Vetter, W.; Santos, F.J.; Neels, H.; Storelli, A.; Storelli, M.M.;  
350 2008. Anthropogenic and naturally occurring Organobrominated compounds in two Deep-Sea  
351 fish species from the Mediterranean. *Environ. Sci. Technol.* 42, 8654–8660.  
352 <http://dx.doi.org/10.1021/es8016528>.

353 Cutshall, N.H.; Larsen, I.L.; Olsen, C.R. ; 1983. *Nucl. Instr. and Meth.*, 206, p. 309.

354 Fabres, J.; Tesi, T.; Velez, J.; Batista, F.; Lee, C.; Calafat, A.; Heuss- ner, S.; Palanques, A.; and  
355 Miserocchi, S.; 2008. Seasonal and event- controlled export of organic matter from the shelf  
356 towards the Gulf of Lions continental slope, *Cont. Shelf Res.*, 28, 1971– 1983.

357 Fernandez-Arcaya U.; Ramirez-Llodra E.; Aguzzi J.; Allcock A. L.; Davies Jaime S.; Dissanayake  
358 Awantha, Harris P.; Howell K.; Huvenne Veerle A. I.; Macmillan-Lawler M.; Martín J.; Menot L.;  
359 Nizinski M.; Puig P.; Rowden Ashley A.; Sanchez F.; Van den Beld Inge M. J.; 2017. Ecological  
360 Role of Submarine Canyons and Need for Canyon Conservation: A Review. *Frontiers in Marine*  
361 *Science* 4, 1-5.

362 Froescheis, O.; Looser, R.; Cailliet, G.M.; Jarman,W.M.; Ballschmiter, K.; 2000. The deep sea as a  
363 final global sink of semivolatile persistent organic pollutants? Part I: PCBs in surface and  
364 deep-sea dwelling fish in the North and South Atlantic and the Monterey Bay Canyon  
365 (California). *Chemosphere* 40, 661–670. [http://dx.doi.org/10.1016/S0045-6535\(99\)00462-2](http://dx.doi.org/10.1016/S0045-6535(99)00462-2).

366 Garcia-Orellana, J.; Sanchez-Cabeza, J.A.; Masqué, P.; Àvila, A.; Costa, E.; Loÿe-Pilot, M.D.;  
367 Bruach-Menchén, J.M.; 2006. Atmospheric fluxes of <sup>210</sup>Pb to the western Mediterranean Sea  
368 and the Saharan dust influence. *J. Geophys. Res. Atmos.* 111, 1–9. doi:10.1029/2005JD006660.

369 Hancock, G.; Edgington, D.N.; Robbins, J.; Smith, J.N.; Brunskill, G.; Pfitzner, J.; 2000. Workshop  
370 on radiological techniques in sédimentation studies: methods and applications 19.  
371 IAEA; 2004. Sediment distribution coefficients and concentration factors, for biota in the  
372 marine environment. International Atomic Energy Agency. Technical report, series 422,  
373 Vienna, Austria.

374 IHO—International Hydrographic Organization; 2008. IHO Standards for Hydrographic  
375 Surveys. Special Publication, 44. Published by the International Hydrographic Bureau, Monaco,  
376 pp. 28.

377 Jamieson, A.J.; Malkocs, T.; Piertney, S.B.; Fujii, T.; Zhang, Z.; 2017. Bioaccumulation of  
378 persistent organic pollutants in the deepest ocean fauna. *Nat. Ecol. Evol.* 1, 1–4. [http://dx.](http://dx.doi.org/10.1038/s41559-016-0051)  
379 [doi.org/10.1038/s41559-016-0051](http://dx.doi.org/10.1038/s41559-016-0051).

380 Kalb, C.; 2008. I sedimenti superficiali della Piattaforma interna del Golfo di Cagliari. Relazioni  
381 tra moto ondoso, correnti indotte e processi di sedimentazione su sistemi di spiaggia  
382 campione. PhD Thesis, Università degli Studi di Cagliari, pp. 295.

383 Khripounoff, A.; Crassous, P.; Lo Bue, N.; Dennielou, B.; Silva Jacinto, R.; 2012. Different types  
384 of sediment gravity flows detected in the Var submarine canyon (northwestern  
385 Mediterranean Sea). *Prog. Oceanogr.*, 106, 138-153.

386 Lecca L.; Panizza V.; Pisano S.; 1998. The sedimentary framework of Cagliari Basin: a Plio-  
387 Quaternary underfed rift basin in the southern Sardinia margin. *Il Quaternario Italian Journal*  
388 *of Quaternary Sciences*, 11(2), 301-318.

389 Lecroart, P.; Maire, O.; Schmidt, S.; Grémare, A.; Anschutz, P.; Meysman, F.J.R.; 2010.  
390 Bioturbation, short-lived radioisotopes, and the tracer-dependence of biodiffusion coefficients.  
391 *Geochim. Cosmochim. Acta* 74, 6049–6063. doi:10.1016/j.gca.2010.06.010.

392 Ligeró, R.; Barrera, M.; Casas-Ruiz, M.; Sales, D.; López-Aguayo, F., 2002. Dating of marine  
393 sediments and time evolution of heavy metal concentrations in the Bay of Cádiz, Spain.  
394 *Environ. Pollut.* 118, 97–108. doi:10.1016/S0269-7491(01)00209-3.

395 Lohmann, R.; Breivik, K.; Dachs, J.; Muir, D.; 2007. Global fate of POPs: current and future  
396 research directions. *Environ. Pollut.* 150, 150–165.  
397 <http://dx.doi.org/10.1016/j.envpol.2007.06.051>.

398 Masqué, P.; Sanchez-Cabeza, J.A.; Bruach, J.M.; Palacios, E.; Canals, M.; 2002. Balance and  
399 residence times of <sup>210</sup>Pb and <sup>210</sup>Po in surface waters of the northwestern Mediterranean  
400 Sea. *Cont. Shelf*. 22, 2127–2146. doi:10.1016/S0278-4343(02)00074-2.

401 Meleddu, A.; Deiana, G.; Paliaga, E.M.; Todde, S.; Orrù, P.E.; 2016. Continental shelf and slope  
402 geomorphology: marine slumping and hyperpycnal flows (Sardinia Southern continental  
403 margin, Italy). *Geogr. Fis. Dinam. Quat.* 39, 183-192, DOI 10.4461/ GFDQ 2016.39.

404 Micallef, A.; Ribó, M.; Canals, M.; Puig, P.; Lastras, G.; Tubau, X.; 2014. Space-for-time  
405 substitution and the evolution of a submarine canyon-channel system in a passive  
406 progradational margin. *Geomorphology*, 221, 34-50.

407 Munsell, A.H.; 1994. *Munsell Soil Color Charts*. Rev. ed. Gretag Macbeth, NewWindsor, NY.

408 Nieuwenhuize, J.; Maas, Y.E.M.; Middelburg, J.J.; 1994. Rapid analysis of organic carbon and  
409 nitrogen in particulate materials. *Mar. Chem.* 45, 217-224.

410 Orrù, P.E.; Deiana, G.; Meleddu, A.; Paliaga, E.; Todde, S.; 2014. Movimenti di massa in scarpata  
411 superiore del Margine meridionale sardo, controllo tettonico e dinamica evolutiva (Golfo di  
412 Cagliari - Sardegna Meridionale). Poster. URL [http://www.ritmare.it/area-](http://www.ritmare.it/area-download/category/34-workshop-ritmare-bologna-2014?download=138:05-orru-et-al-sp4)  
413 [download/category/34-workshop-ritmare-bologna-2014?download=138:05-orru-et-al-sp4](http://www.ritmare.it/area-download/category/34-workshop-ritmare-bologna-2014?download=138:05-orru-et-al-sp4).

414 Pham, M.K.; Povinec, P.P.; Nies, H.; Betti, M.; 2013. Dry and wet deposition of <sup>7</sup>Be, <sup>210</sup>Pb and  
415 <sup>137</sup>Cs in Monaco air during 1998-2010: Seasonal variations of deposition fluxes. *J. Environ.*  
416 *Radioact.* 120, 45–57.

417 Piper, D.J.W.; Normark, W.R.; 2009. Processes that initiate turbidity currents and their  
418 influence on turbidites: a marine geology perspective. *J. Sediment. Res.*, 79, 347-362.

419 Puig P.; Palanques A.; Martín J.; 2014. Contemporary sediment-transport processes in  
420 submarine canyons. *Annu. Rev. Mar. Sci.*, 6, 53-77.

421 Puig, P.; Durán, R.; Muñoz, A.; Elvira, E.; Guillén, J.; 2017. Submarine canyon-head  
422 morphologies and inferred sediment transport processes in the Alías-Almanzora canyon  
423 system (SW Mediterranean): On the role of the sediment supply. *Marine Geology*, 393, 21-34.

424 Robbins, J.A.; 1978. Geochemical and geophysical applications of radioactive lead isotopes, in:  
425 Nriagu, J.O. (Ed.), *Biochemistry of Lead*. Elsevier.

426 Robbins, J.A.; Edgington, D.N.; 1975. Determination of recent sedimentation rates in Lake  
427 Michigan using Pb-210 and Cs-137. *Geochim. Cosmochim. Acta* 39, 285–304.  
428 doi:10.1016/0016-7037(75)90198-2.

429 Scheringer, M.; Jones, K.C.; Matthies, M.; Simonich, S.; van de Meent, D.; 2009. Multimedia  
430 partitioning, overall persistence, and long-range transport potential in the context of POPs  
431 and PBT chemical assessments. *Integrated Environmental Assessment and Management* 5,  
432 557–576.

433 Shepard, R.P.; 1981. Submarine canyons: multiple causes and long-time persistence. *Am.*  
434 *Assoc. Pet. Geol. Bull.*, 65, 1062-1077.

435 Smith, J.N.; 2001. Why should we believe <sup>210</sup>Pb sediment geochronologies? *J. Environ.*  
436 *Radioact.* 55, 121–123. doi:10.1016/S0265-931X(00)00152-1.

437 Storelli, M.M.; Losada, S.; Marcotrigiano, G.O.; Roosens, L.; Barone, G.; Neels, H.; Covaci, A.;  
438 2009. Polychlorinated biphenyl and organochlorine pesticide contamination signatures in  
439 deep-sea fish from the Mediterranean Sea. *Environ. Res.* 109:851–856.  
440 <http://dx.doi.org/10.1016/j.envres.2009.07.008>.

441 Talling, P.J.; 2014. On the triggers, resulting flow types and frequencies of subaqueous  
442 sediment density flows in different settings. *Mar. Geol.*, 352, 155-182.

443 US-EPA (Environmental Protection Agency); 2007. Method 7473. Mercury in Solids and  
444 Solutions by Thermal Decomposition, Amalgamation, and Atomic Absorption  
445 Spectrophotometry.



446 van Beek, P.; Sternberg, E.; Reyss, J.-L.; Souhaut, M.; Robin, E.; Jeandel, C.; 2009.  $^{228}\text{Ra}/^{226}\text{Ra}$   
447 and  $^{226}\text{Ra}/\text{Ba}$  ratios in the Western Mediterranean Sea: Barite formation and transport in the  
448 water column. *Geochim. Cosmochim. Acta* 73, 4720–4737. doi:10.1016/j.gca.2009.05.063.

449 van Wijngaarden, S. J.; Steeneken, H. J. M.; and Houtgast, T.; 2002. Quantifying the  
450 intelligibility of speech in noise for nonnative listeners. *J. Acoust. Soc. Am.* 111(4), 1906–1916.

451 Waples, J.T.; Benitez-Nelson, C.; Savoye, N.; Rutgers van der Loeff, M.; Baskaran, M.; Gustafsson,  
452 Ö.; 2006. An introduction to the application and future use of  $^{234}\text{Th}$  in aquatic systems. *Mar.*  
453 *Chem.* 100, 166–189. doi:10.1016/j.marchem.2005.10.011.

454

## 455 **Figure captions**

456 **Figure 1** A) Location Map of Gulf of Cagliari. B) Digital Terrain Model (DTM) of the SE sector  
457 of Sardinia. CG= Gulf of Cagliari; BK=Banghittu Knoll; A-TT=Algerian-Tyrrhenian Trough;  
458 CR=Carbonara Ridge; CV=Carbonara Valley; SPC, PC, SC and SEC=Spartivento, Pula, Sarroch  
459 and San’Elia-Foxi canyons. White capital letters are locations of sampling stations. C)  
460 Elevation profile extracted from the DTM (location is in B).

461 **Figure 2** A) and B)  $\Sigma\text{PAHs}$ ,  $\Sigma\text{PCBs}$ , Hg, As and Pb concentrations vs age in the A2TM and A3TM  
462 sediment cores. Box-whisker plot of silt fraction subdivided in three time intervals (values  
463 in %), is also reported for A2TM sediment core. C), D) and E)  $\Sigma\text{PAHs}$ ,  $\Sigma\text{PCBs}$ , Hg, As and Pb  
464 concentrations vs depth in the A4TM, A6TM and A7TM. Grey bands marks the presence of  
465  $^{137}\text{Cs}$  released in the last 60 years.

466 **Figure 3** A) Map showing the distances from Cagliari (which is the main source of sediments  
467 in the Gulf of Cagliari) to the sampling stations (A2TM, A3TM, A4TM and A6TM) and the  
468 distance vs derived  $^{137}\text{Cs}$  Inventory plot (B). C) “Morphologic distance” (i.e. the true distance  
469 covered by sediments) calculated taking into account the morphology of the seafloor and its  
470 corresponding higher fitting distance vs  $^{137}\text{Cs}$  Inventory plot (D).

471 **Figure 4** The “morphologic distance”, previously mentioned, vs  $^{137}\text{Cs}$  Inventory calculated  
472 considering its terrigenous component (i.e. by subtracting A7TM value) and Hg and Zn  
473 “normalised” inventories (see text for further details) for A2TM, A3TM, A4TM and A6TM.

474 **Figure 5**  $^{137}\text{Cs}$  inventories vs  $\Sigma\text{HPAHs}$ ,  $\Sigma\text{PCBs}$ , Hg, Cu, Zn and Pb plots for all sampling stations.  
475

## 476 **Table captions**

477 **Table 1** Table of coordinates and water depth of the studied sediment cores together with  
478 sampling site and core length (cm).

479 **Table 2** Inventories values of  $^{210}\text{Pb}$ ,  $^{137}\text{Cs}$ ,  $\Sigma\text{HPAHs}$ ,  $\Sigma\text{PCBs}$  and TEs for the studied sediment  
480 cores.

481

## 482 **Supplementary Figures**

483 **Figure S1**  $^{210}\text{Pb}$  and  $^{137}\text{Cs}$  activity profiles of A2TM, A3TM, A4TM, A6TM, A7TM sediment  
484 cores collected in the SE Sardinia with indication of water depth (m).

485 **Figure S2** Comparison between the measured and the estimated value of  $^{210}\text{Pb}_{\text{xs}}$  flux at the  
486 water-sediment interface for the studied sediment cores.  $F_a + F_m$  = atmospheric + water  
487 production  $^{210}\text{Pb}_{\text{xs}}$  flux;  $F_s$  = sediment water interface  $^{210}\text{Pb}_{\text{xs}}$  flux.

488 **Figure S3** On the left is shown the slope map derived by the DTM of Cagliari, while the right  
489 part of the figure displays the flow patterns of sediments.

490 **Figure S4** Profiles of grain size composition vs depth (cm).

491

## 492 **Supplementary Tables**

493 **Table S1** Mean values of Al, Fe, Mn Cd, Pb, Co, V, As, Cr, Cu, Ni, Zn, Hg, TOC, TN,  $\Sigma\text{PAH}$  and  
494  $\Sigma\text{PCB}$ .

495 **Table S2** Mean values activity of  $^{226}\text{Ra}$ ,  $^{40}\text{K}$ , and supported  $^{234}\text{Th}$  ( $\text{Bq kg}^{-1}$ , dry weight).  $^{234}\text{Th}$ s  
496 downcore mass-depth with in square brackets the depth value in cm.  $^{210}\text{Pb}$ s and  $^{137}\text{Cs}$   
497 inventories are also reported.

Table 1

[Click here to download Table: Table\\_1\\_2mag18.pdf](#)

Area	ID station	Latitudine N	Longitudine E	Depth mbsl	Legth cm
<b>Gulf of Cagliari</b> (Sant'Elia-Foxi Canyon; SEC)	<b>A2TM</b>	39°05'34"	09°21'29"	625	33
<b>Gulf of Cagliari</b> (Sarroch Canyon; SC)	<b>A3TM</b>	39°00'21"	09°18'00"	636	36
<b>Gulf of Cagliari</b> (Carbonara Canyon; CC)	<b>A4TM</b>	38°59'01"	09°29'22"	907	28
<b>Gulf of Cagliari</b> (Pula Canyon; PC)	<b>A6TM</b>	38°46'05"	09°12'07"	787	29
<b>SE Sardinia</b> (Trough;A-TT)	<b>A7TM</b>	38°43'29"	09°40'36"	1153	22

Table 2

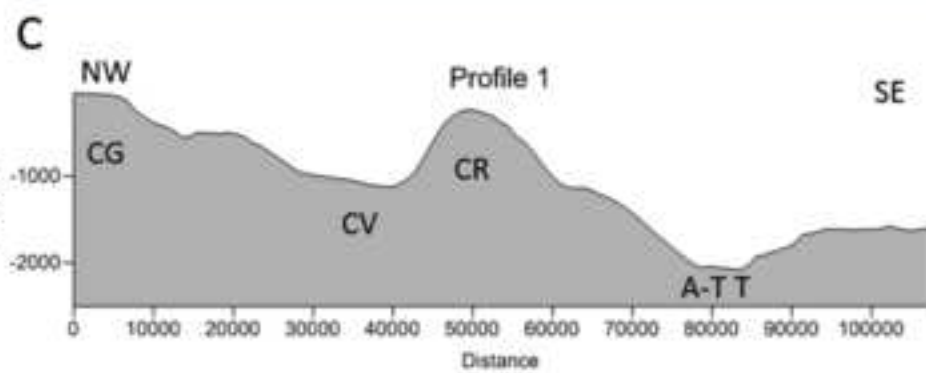
[Click here to download Table: Table\\_2\\_2mag18.pdf](#)

Inventory	$^{137}\text{Cs}$ Bq m <sup>-2</sup>	$\Sigma\text{HPAHs}_{\text{antr}}$ mg m <sup>-2</sup>	$\Sigma\text{PCBs}_{\text{antr}}$ $\mu\text{g m}^{-2}$	$\text{Hg}_{\text{antr}}$ $\mu\text{g m}^{-2}$	$\text{V}_{\text{antr}}$ mg m <sup>-2</sup>	$\text{Cu}_{\text{antr}}$ mg m <sup>-2</sup>	$\text{Pb}_{\text{antr}}$ mg m <sup>-2</sup>	$\text{Zn}_{\text{antr}}$ mg m <sup>-2</sup>	$\text{As}_{\text{antr}}$ mg m <sup>-2</sup>	$\text{Cd}_{\text{antr}}$ mg m <sup>-2</sup>	$\text{Co}_{\text{antr}}$ mg m <sup>-2</sup>	$\text{Cr}_{\text{antr}}$ mg m <sup>-2</sup>	$\text{Ni}_{\text{antr}}$ mg m <sup>-2</sup>
A2TM	740	4.6	66	9724	6019	1077	5004	6250	2165	45	474	2961	1351
A3TM	560	1.6	37	5614	2357	657	1600	2903	628	24	182	1482	617
A4TM	450	1.2	4.1	2724	2491	424	1153	1758	1929	28	205	1759	576
A6TM	360	0.8	5.3	2572	938	292	693	731	816	24	136	730	553
A7TM	110	0.3	2.4	994	146	129	402	251	244	3	43	127	75

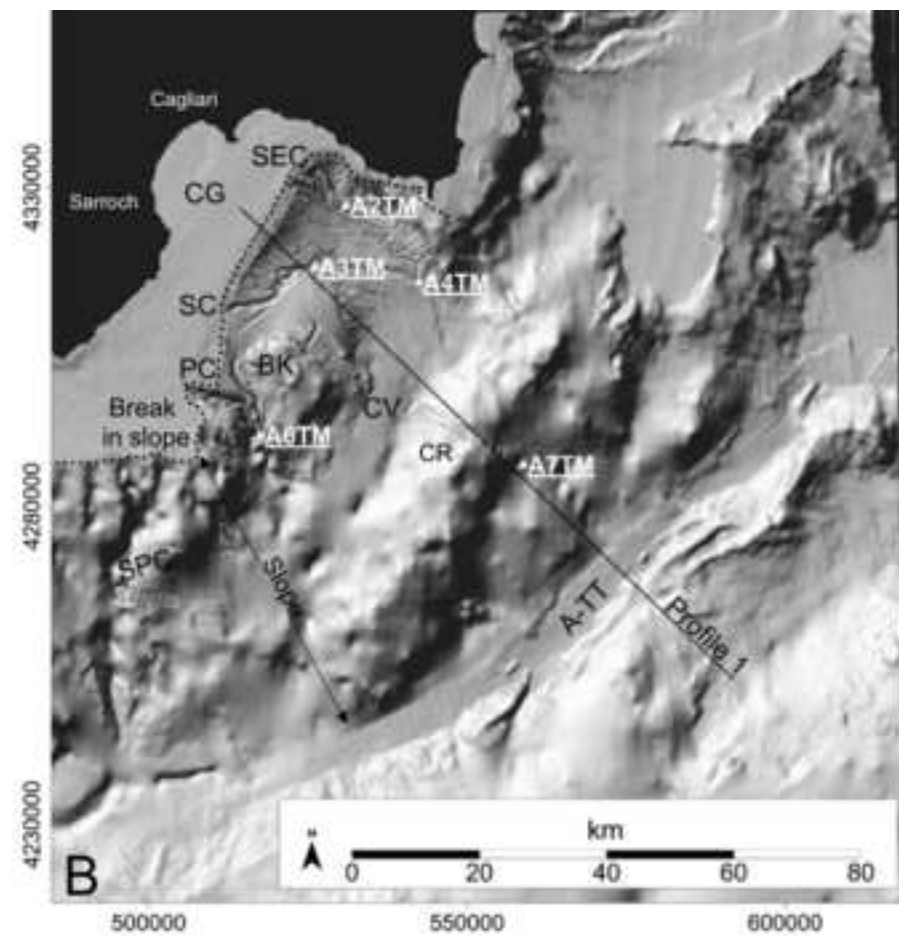
Figure 1  
[Click here to download high resolution image](#)



A



C



B

Figure 2  
[Click here to download high resolution image](#)

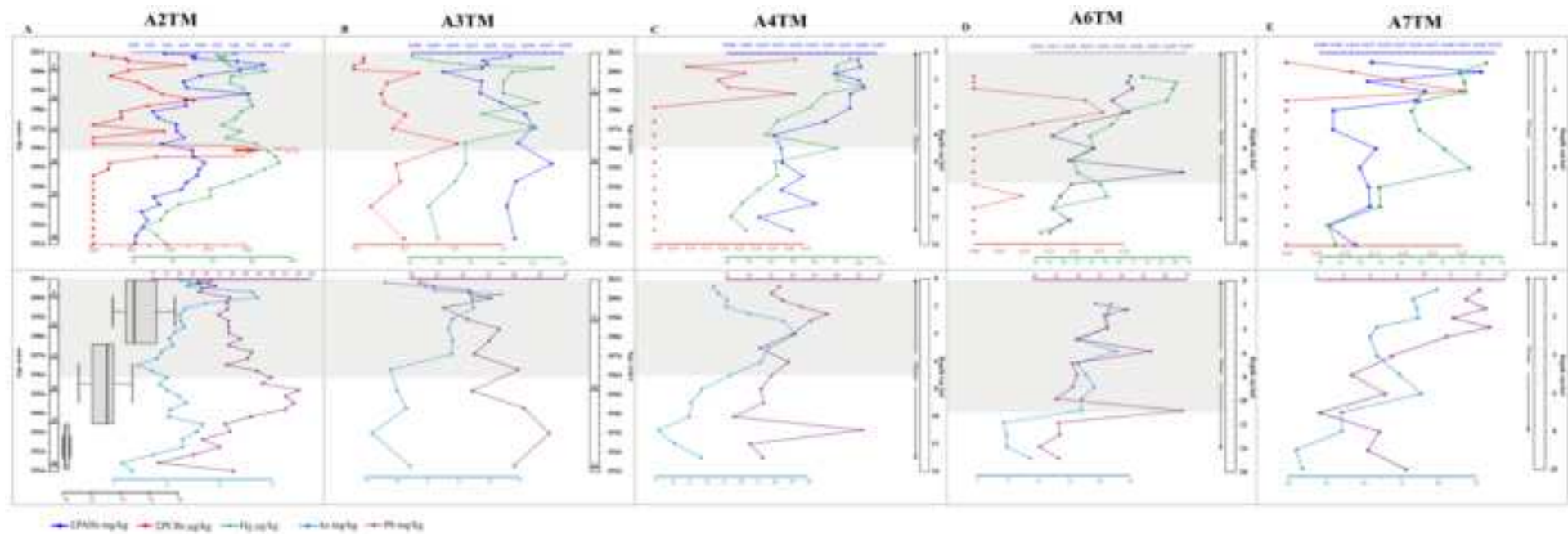


Figure 3  
[Click here to download high resolution image](#)

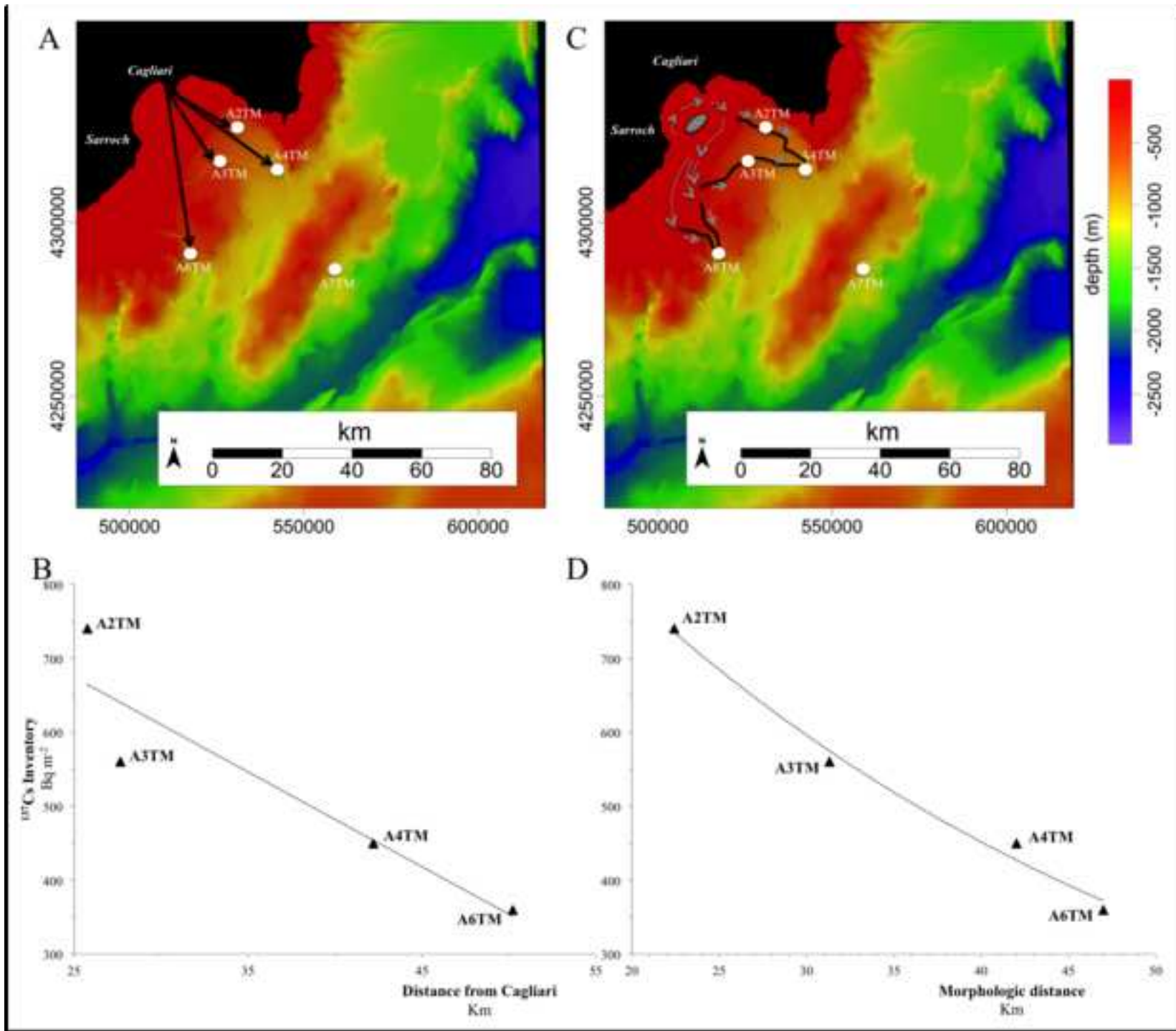




Figure 4  
[Click here to download high resolution image](#)

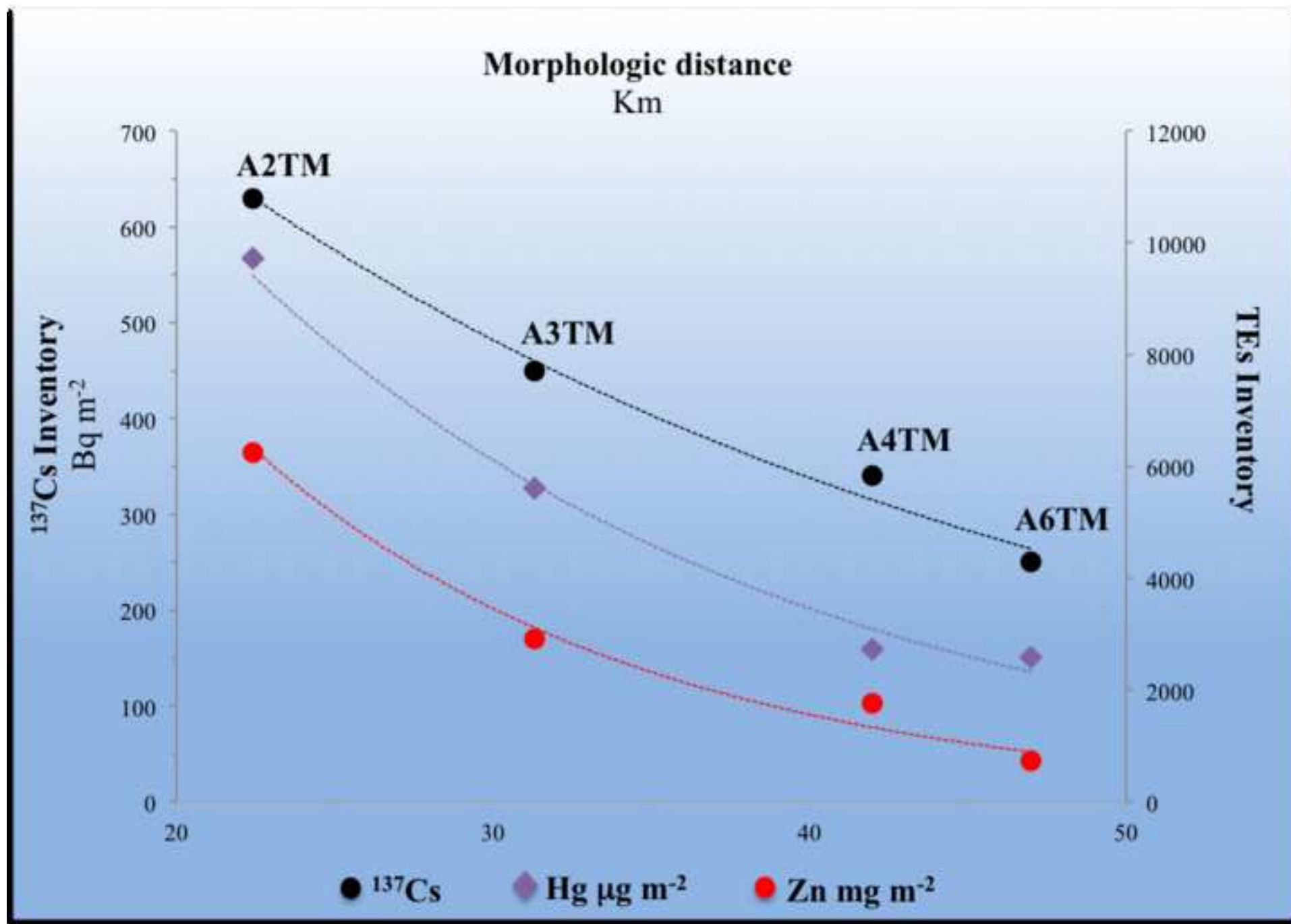
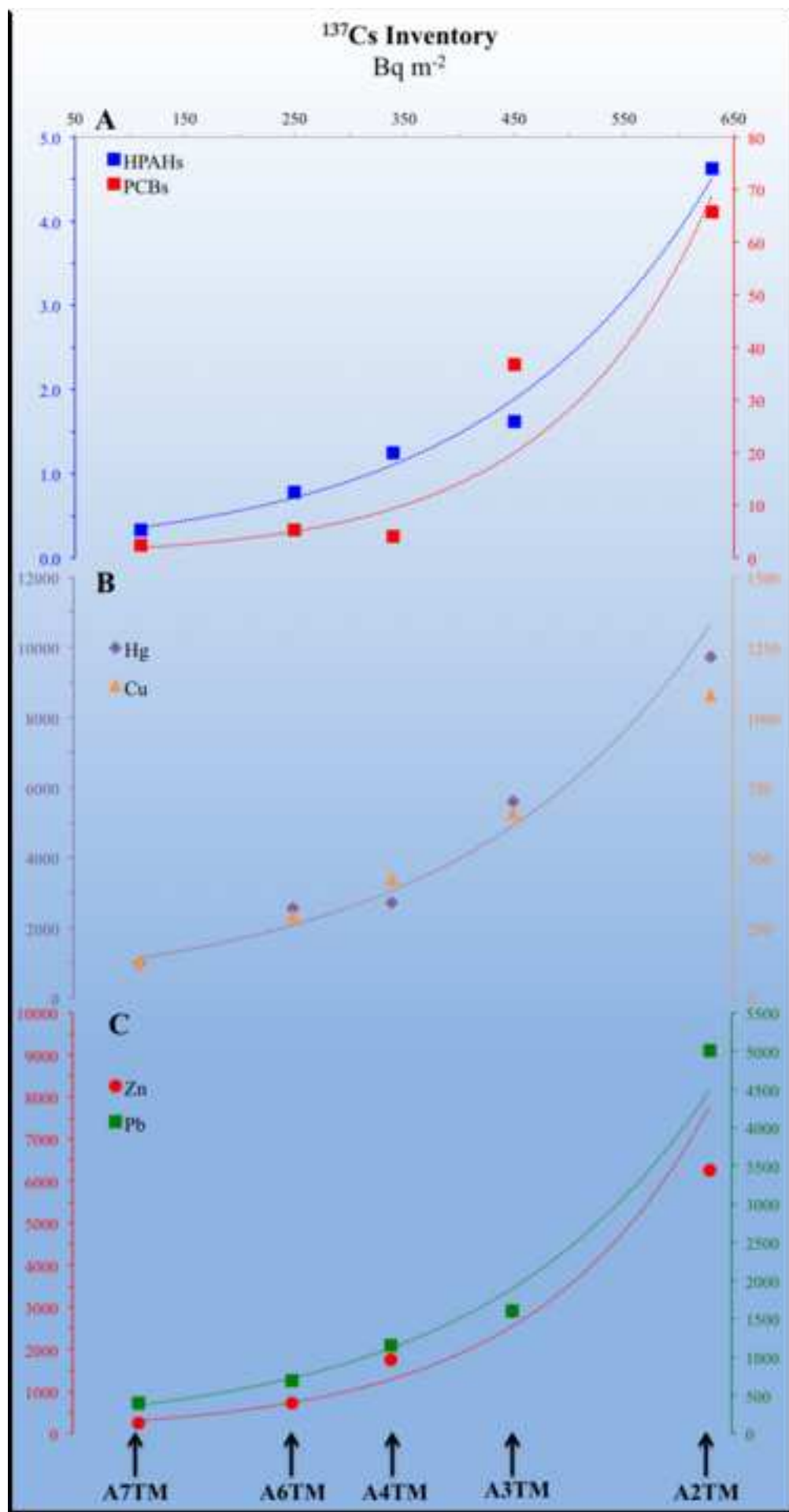


Figure 5  
[Click here to download high resolution image](#)



**Supplementary material - Information**

**[Click here to download Supplementary material for on-line publication only: Supplementary Matarial\\_2mag18.docx](#)**

**Supplementary material - Table S1**

[Click here to download Supplementary material for on-line publication only: Table\\_S1\\_2mag18.pdf](#)

**Supplementary material - Table S2**

[Click here to download Supplementary material for on-line publication only: Table\\_S2\\_2mag18.pdf](#)

**Supplementary material - Figure S1**

[Click here to download Supplementary material for on-line publication only: Supplementary S1\\_2mag18.png](#)

**Supplementary material - Figure S2**

[Click here to download Supplementary material for on-line publication only: Supplementary S2\\_2mag18.png](#)

**Supplementary material - Figure S3**

[Click here to download Supplementary material for on-line publication only: Supplementary S3\\_2mag18.png](#)



**Supplementary material - Figure S4**

[Click here to download Supplementary material for on-line publication only: Supplementary S4\\_2mag18.png](#)